Quantitative evaluation of equatorial small-angle X-ray scattering for cylindrical fibers*

Li Xiao-Yun(李小芸), Li Xiu-Hong(李秀宏), Yang Chun-Ming(杨春明), Hua Wen-Qiang(滑文强), Zhao Nie(赵 镍), Miao Xia-Ran(缪夏然), Tian Feng(田 丰), Wang Yu-Zhu(王玉柱), Bian Feng-Gang(边风刚), and Wang Jie(王 劼)†

Shanghai Synchrotron Radiation Facility, Shanghai Institute of Applied Physics, Chinese Academy of Sciences, Shanghai 201204, *China*

(Received 3 September 2012; revised manuscript received 31 October 2012)

Elongated microvoids, internal fibrillar structure, and edge scattering from both surface refraction cause an equatorial streak in small angle X-ray scattering. A model for analyzing the edge scattering of fibers is proposed. Simulation results indicate that the intensity of edge scattering from surface refraction of a cylindrical fiber is strong and makes an important contribution to the equatorial streak. Two factors influence edge scattering intensity. One is the sample-to-detector distance (D); edge scattering intensity increases with increasing D. The equatorial streak becomes weak when D is shortened. The other factor is the refraction index. Edge scattering intensity increases as the real component of the refraction index decreases. In experiment, weak or even no equatorial streaks were found for samples measured in a roughly index-matching fluid. Edge scattering can be eliminated or weakened, and it can be calculated by comparing the intensities of a cylindrical fiber when it is measured in air and in index-matching fluid. The simulation data are basically in agreement with the experimental data.

Keywords: fiber, edge scattering, small angle scattering, equatorial streak

PACS: 61.05.cf, 41.60.Ap **DOI:** 10.1088/1674-1056/22/4/046102

1. Introduction

Small angle X-ray scattering (SAXS) is an analytical technique that can be used to study microstructures at a nanometer scale in material science.[1–4] And it can be used in analyzing the microporosity of fibers. SAXS patterns from natural or synthetic fibers exhibit a sharp streak along the equator (perpendicular to the fiber axis). The equatorial streak is normally attributed to elongated voids within the fiber or fibrillar structure.[5–9] Ruland proposed that polyacrylonitrile fibers contain some cylindrical microvoids, and he calculated small-angle scattering intensity. The calculated small-angle scattering intensity shows that there is also an equatorial streak perpendicular to the fiber axis.[10] So far, for polyacrylonitrile and cellulose fibers, equatorial streaks have been ascribed to void content.[4,10–16] And the streaks have also been detected by TEM and SEM.[17,18] For Kevlar fiber, most researchers take microfibrils to be the source of the equatorial streaks.[19–21] Benjamin S. Hsiao and his coworkers reported that during different conditions, deformations of polyvinylidene fluoride fiber of equatorial streaks were attributed to the formation of microfibrils or microvoids.[22] The equatorial streak of fibers with high take-up speed under zero or small strain is attributed to voids. The equatorial streak observed in fibers under high strain at all take-up speeds is attributed to microfibrils. And the dimensions of the lengths of microfibrils and microvoids were estimated by Ruland's method.[10] In D. T. Grubb's study of Nylon-6 fibers during dehydration, the authors demonstrated that the equatorial streak is due to surface refraction. If the beam size is smaller than the fiber diameter, there is no equatorial streak when the beam is incident on the center of the fiber. Otherwise, the edge of the fiber will cause a strong equatorial streak.[23] On-axis microbeam wide- and small-angle scattering was used to study different sections of poly (*p*-phenylene terephthalamide) fiber, it was found that the equatorial streak appeared when the microbeam irradiated the edge of fiber (skin of the fiber).[24] From the present studies, it can be concluded that there are several contributions to an equatorial streak, including the microfibrillar structure, elongated voids, and edge scattering intensity from surface refraction and reflection. The equatorial streak of SAXS patterns measured in the air contains the contribution of edge scattering intensity. However edge scattering intensity does not reveal information about the microstructure of the inner fiber, but provides only information about the surface of the fiber. So the character of the microstructure is not so exact. Some information reflected from the inner fiber was masked by the strong intensity of edge scattering.[25] Edge scattering has a great effect on the scattering pattern, especially for the Guinier region. So edge scattering should be eliminated in order to obtain a clear Guinier region which reflects the size of the whole scattering object, not just the interface.

In 1986, M. P. Hentschel observed equatorial small angle scattering of Cu $K\alpha$ radiation, which was caused by both reflection and refraction.[26] For any material, at X-ray wave-

*Project supported by the National Natural Science Foundation of China (Grant Nos. 50903089, 10979073, 11005143, and 10979006) and the National Basic Research Program of China (Grant Nos. 2010CB934501, 2011CB606104, and 2011CB605604).

†Corresponding author. E-mail: wangjie@sinap.ac.cn

© 2013 Chinese Physical Society and IOP Publishing Ltd

lengths, the refraction index is close to one. The critical angle θ_c of total reflection is about 10^{-3} arc. The intensity of the deflected X-rays falls nearly to zero at the critical angle of total reflection.[27] But for small angle scattering, the reflection and refraction intensity of the deflected X-rays cannot be blocked by the beamstop. So it affects the signal that comes from the inner structure. Gupta *et al*.[28] reported that the intensity of edge scattering arising from refraction can be measured if a sample is immersed in a roughly index-matching fluid. However, for some *in-situ* measurements, this method is restrictive. So evaluating edge scattering intensity arising from reflection and refraction is necessary; but most researchers neglect the contributions of edge scattering intensity when analyzing data. In this work a model based on reflection and refraction is set up to evaluate edge scattering intensity. The model is described in Subsection 3.1. The relationship of the intensity of reflection, refraction and refraction indexes, and sample-to-detector distance is established in this paper. Our aim is to find a way to eliminate the intensity of edge scattering in the equatorial streak from the SAXS pattern.

2. Experimental section

2.1. Sample preparation

The carbon fiber (Sample a1), polyethylene terephthalate (PET) fiber (Sample b1), and high density polyethylene (HDPE) fiber (Sample c1) were chosen for the experiment. The properties of the samples are listed in Table 1. According to $\delta \approx \rho \cdot \lambda^2$, it is obvious that the electron density of PET and HDPE fibers is similar to that of C_2H_5OH. Here carbon fiber was used as a contrasting sample and it is discussed in Section 4.

Table 1. Characteristics of carbon, PET, HDPE fiber, and C_2H_5OH.

Sample code	Density(g/cm^3)	Refraction index[29] $n = 1-\delta-i\beta$ (10^4 eV)	
		$\delta/10^{-6}$	$\beta/10^{-9}$
Carbon fiber	1.80	4.00	4.00
PET fiber	1.38	2.00	4.20
HDPE fiber	0.95	2.05	1.85
C_2H_5OH	0.79	2.00	25

2.2. SAXS measurements

SAXS measurement was performed on beamline BL16B1 using a three-slit system at Shanghai Synchrotron Radiation Facility. An energy resolution of 6×10^{-4} was obtained from a water-cooled Si (111) double-crystal monochromator. The wavelength of the X-ray was 0.124 nm. The 2D SAXS patterns were recorded by a Mar165 CCD at a resolution of 2048×2048 pixels and a pixel size of 80 μm×80 μm for quantitative analysis. The sample-to-detector distance was 5160 mm for SAXS (calibrated by beef tendon standard).

All samples were mounted on a rectangular hollow metal frame. Every filament was stretched tightly. In our experiments, the thickness of the fiber sample is the same before and after the addition of solvent. First, Sample a1, Sample b1, and Sample c1 were measured in the air with exposure times of 20 s, 30 s, and 200 s, respectively. Then, Sample a1, Sample b1, and Sample c1, together with the frame holding the samples, were immersed in a cell with a particular solvent whose electron density is close to that of the fibers (named Sample a2, Sample b2, and Sample c2, respectively). The cell was sealed using Kapton film.

2.3. Data processing

Data evaluation of the SAXS patterns was performed with Matlab R2009. At first, the two-dimensional patterns obtained from different measurement environments needed the background scattering subtracted. Next, the exposure time and scattering intensity were normalized. Then, in experiment, the intensity of the edge scattering caused by reflection and refraction of X-rays from the surface of the fiber was obtained by subtracting the scattering intensity of the sample as measured in a particular solvent from that as measured in air.

3. Data evaluation of edge scattering

3.1. Model

According to the present experimental conditions of the BL16B1 beamline in SSRF, a function as follows was used to describe the distribution of the incident intensity:

$$I_i(x,z) = I_{0x} I_{0z} \exp\left(-\frac{(z_1-z_0)^2}{2\sigma_z^2}\right), \tag{1}$$

where $I_i(x,z)$ is the distribution of primary incident intensity, I_{0x} and I_{0z} are the intensity at x and z centers, respectively. σ_z is the full width at half maximum of the intensity in the z direction. The fiber was assumed to be a smooth cylinder with radius R. The refractive index of X-rays is $n = 1-\delta-i\beta$, $\delta \approx \rho \cdot \lambda^2$,[24] $\delta = c \times 10^{-6}$ which is very small. (c is determined by specimen, λ is the wavelength of X-rays, ρ is the contrast of electron density.) According to the law of total reflection, the angle of α_c can be calculated. α_c is defined as the "critical angle" of total reflection. Therefore, in θ ($0 \le \theta \le \alpha_c$), X-ray reflection occurs. In the range of the complementary angle ($\pi/2-\theta$), X-ray refraction occurs.

We assumed that all filaments aligned regularly along the z direction. Neglecting absorption, the intensity of reflection $I_{\text{reflection}}$ can be expressed as[26]

$$I_{\text{reflection}} = \begin{cases} C \cdot I_i(x_1,z_1) \cdot R \cdot \sin\theta, & |\theta| \le \alpha_c, \\ 0, & |\theta| > \alpha_c. \end{cases} \tag{2}$$

The refracted intensity $I_{\text{refraction}}$ at small angle 2θ was found

to be

$$I_{\text{refraction}} = \begin{cases} C \cdot I_i(x_1, z_1) R\delta^2/\theta^3, & |\theta| \le \alpha_c, \\ 0, & |\theta| > \alpha_c. \end{cases} \quad (3)$$

In Eqs. (2) and (3), θ is the scattering angle, and C is a coefficient.

We take the direction of the incident beam as the y axis, the horizontal direction as the x axis, the vertical direction as the z axis, the center of the beamstop is (0, 0, 0) and the fiber axis is parallel to the z axis (Fig. 1). D is the distance of the sample-to-detector. Because the radius of fibers is far smaller than the sample-to-detector distance, a cross section of one filament can be taken as one point.

The maximum deflection in the x direction is determined by the critical angle of total reflection. That is

$$x_{\max} = D \cdot \tan(2\alpha_c). \quad (4)$$

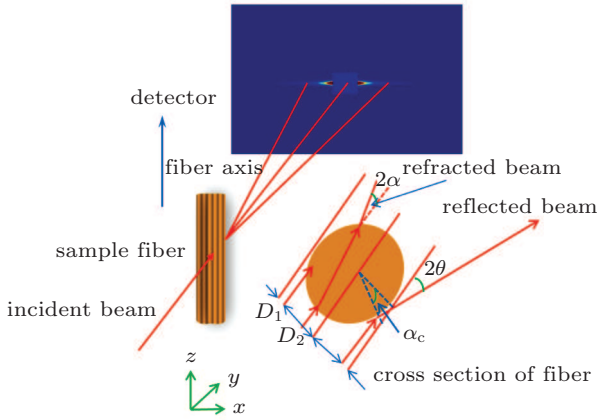


Fig. 1. (color online) Model for small-angle X-ray scattering of cylindrical fiber; D_1 and D_2 are the regions where total reflection and refraction occur, respectively.

3.2. Simulation results

The distribution of incident intensity is shown in Fig. 2. The parameters of the incident beam are as follows:

$$I_0 = I_{ox} \cdot I_{oz} = 2.1 \times 10^9, \quad \sigma_z = 0.8,$$
$$I_{ox} = 4.6 \times 10^4 \text{ /s}, \quad -0.5 \text{ mm} \le x \le 0.5 \text{ mm},$$

where I_0 is the center intensity of the primary incident beam. So we can calculate flux $= 6.15 \times 10^9$ photons/s, which is consistent with the flux in BL16B at SSRF. And the X-ray absorption index of the materials can be obtained in an ionization chamber before and after sample.

Equations (2) and (3) have been used to simulate the edge scattering intensity from reflection and refraction. For a fiber, the critical angle of total reflection is very small, being at mrad level and only a cross section of 10^{-6} of the fiber diameter is involved for reflection; therefore the intensity of reflection can be neglected.[24] The refraction intensity is shown in Fig. 2(b) ($\delta = 4.00 \times 10^{-6}$). The chosen parameters are $R = 25$ μm, $c = 4.0$, and $D = 5160$ mm. In simulation, the size of the beamstop is about 8 mm, which agrees with the experiment. A broad distribution of refraction intensity on the equator is evident. From the simulation shown in Fig. 3, we see that the refraction intensity is strong. And the refraction intensity cannot be neglected because the intensity is strong near the beamstop. When $x = 5$ mm (close to the beamstop) and $z = 0$, the intensity is about 10^4 (Fig. 3). It is easy to see that the refraction intensity makes a great contribution to the equatorial streak of SAXS.

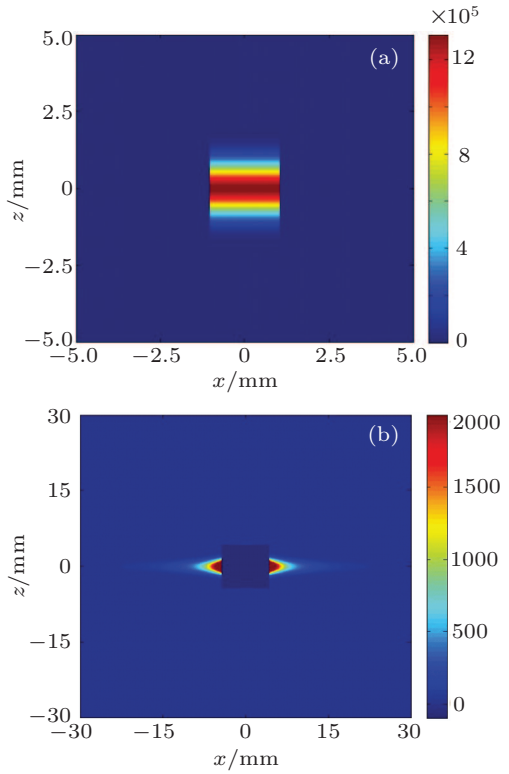


Fig. 2. (color online) (a) The distribution of incident intensity. (b) The distribution of refraction intensity (δ=4.00×10^{-6}); the collection time was 1 s.

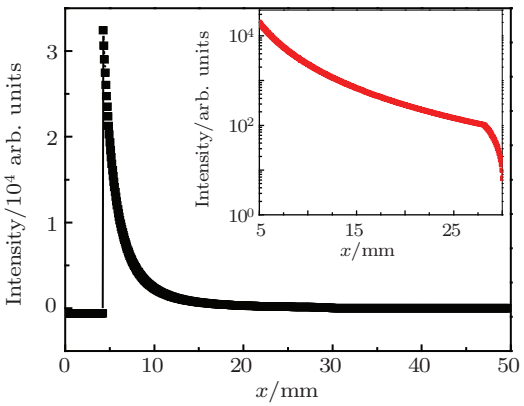


Fig. 3. (color online) The distribution of total intensity at $z = 0$ and $\delta = 4.00 \times 10^{-6}$; the time is 20 s.

3.3. Data evaluation

3.3.1. Influence of sample-to-detector distance

From Eqs. (1) and (2), it is found that the refraction intensity is proportional to the radius for a single fiber. And

from Eq. (4), it can be shown that the sample-to-detector distance determines the angle of the reflected and refracted light deflection at the detector. The maximum deflection distance is proportional to D. So for wide angle scattering of X-rays (WAXS), the reflection and refraction intensities have no influence on the experimental data because the deflection angle is small enough that the reflection and refraction intensities are blocked by the beamstop. For small angle scattering of X-rays (SAXS), the beamstop can only block a part of reflection and refraction intensities, so contributed to the equatorial streak inevitably. A study of the reflection and refraction intensity distribution and sample-to-detector distance of fibers with $\delta = 4.00 \times 10^{-6}$ is presented in this section. Figure 4 shows total intensity at $z = 0$. It is found that total intensity increases with increasing sample-to-detector distance. And the slope of total intensity decreases with increasing sample-to-detector distance. And total intensity decreases dramatically when x is out of the maximum deflection distance but far larger than the incident beam. This indicates the refraction intensity is strong and plays an important role in the equatorial streak. Such a strong, intense streak has been discussed by D. T. Grubb[23] and W. Rungswang.[30]

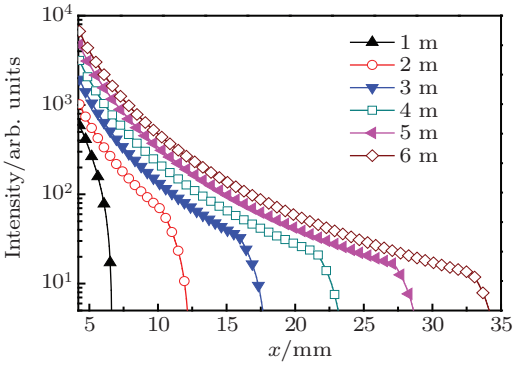


Fig. 4. (color online) The distribution of edge scattering at $z = 0$, $\delta = 4.00 \times 10^{-6}$ with different sample-to-detector distances.

3.3.2. Influence of refraction index

According to the refraction law, the critical angle of total reflection is proportional to the refractive index. The larger the refractive index is, the larger the deflection angle is. The intensity of refraction and reflection distributions will change. Figure 5 shows simulation results for the refraction intensity of carbon fiber ($\delta = 4.00 \times 10^{-6}$) and PE fiber ($\delta = 2.05 \times 10^{-6}$). Comparing the two kinds of fibers, it was found that the distribution of refraction intensity becomes weak as δ decreases.

In order to understand the relationship of edge scattering and δ, edge scattering intensity was calculated for different δ values. Here, taking $z = 0$ for example (Fig. 6), edge scattering intensity decreases with increasing x. It is evident that the total intensity is proportional to δ. The width and the value of the intensity distribution both decrease with decreasing δ. That is to say, a fiber that has a small δ has a small influence on the equatorial streak. It can be concluded that fibers with different δ make different contributions to the equatorial streak. Fibers with high δ make a larger contribution to the equatorial streak.

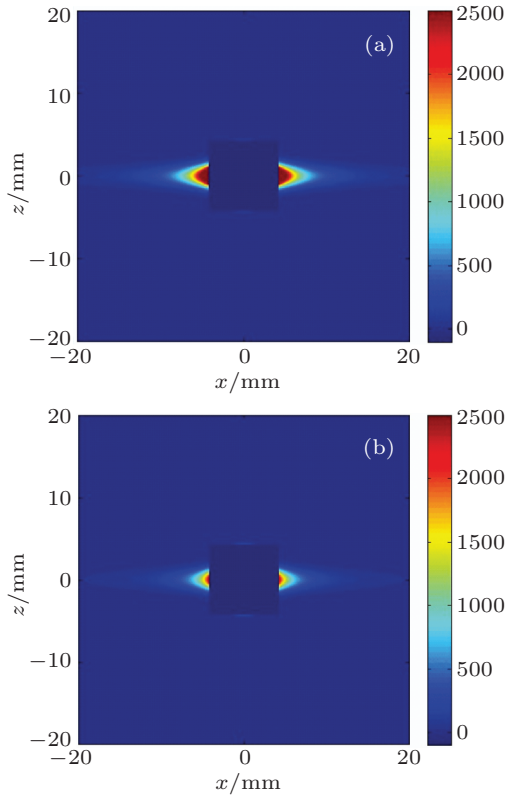


Fig. 5. (color online) Distribution of refraction intensity of (a) carbon fiber, (b) HDPE fiber at the detector plane.

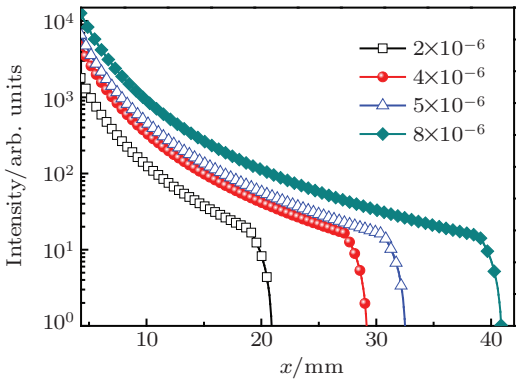


Fig. 6. (color online) The distribution of edge scattering intensity at $z = 0$ with different δ.

3.4. Results and discussion

Figure 7 shows SAXS patterns of three samples: carbon, PET, and HDPE fibers, obtained in two different environments. The patterns in Fig. 7(A) are obtained in air, while the patterns in Fig. 7(B) are obtained in an ethanol-filled chamber. Figure 7(C) shows a pattern derived by subtracting the scattering pattern obtained in ethanol-filed chamber (Fig. 7(B)) from the SAXS pattern obtained in air (as

Fig. 7(C) = Fig. 7(A)–Fig. 7(B)). Strong equatorial streaks are observed in Fig. 7(A), while weak or even no equatorial streaks are found in Fig. 7(B). Since the electronic density of ethanol is close to that of PET and HDPE fibers, the SAXS patterns shown in Figs. 7(b2) and 7(c2) can be considered to be a scattering obtained from the interior structure of the samples because it is impossible that the microstructures of fibers, like fibrillar structure, microvoids, etc., were changed in such a short time.[25] In our experiments, after measuring in air, the same sample was measured in an ethanol-filled chamber immediately. So the equatorial streaks in Figs. 7(b3) and 7(c3) can be considered to be edge scattering from surface refraction of the fibers. In Fig. 7(C), it can be found that the edge scattering intensity of carbon fiber is much longer in the equatorial direction than that of PET and PE fibers. For carbon fiber, the edge scattering can be only partly eliminated because there is also a contrast in electron density between carbon fiber and ethanol. The result indicates that the refraction index δ is one factor which influences the intensity of the equatorial streak. And the intensity increases with increasing δ. This is consistent with our simulation (Fig. 6).

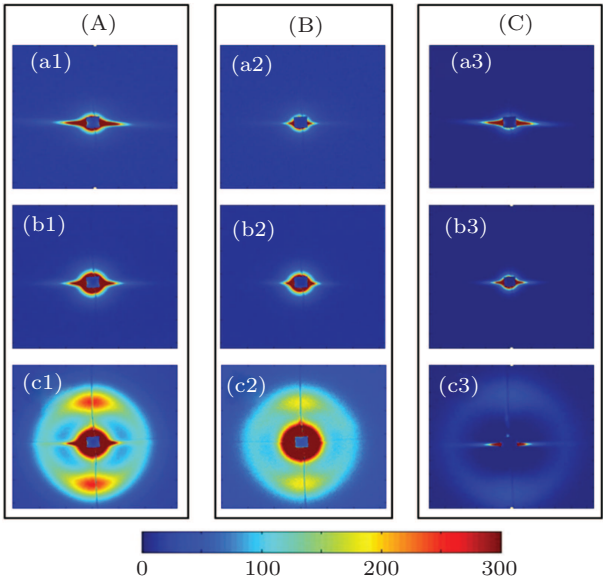


Fig. 7. (color online) SAXS patterns of (a1) and (a2): carbon fiber, (b1) and (b2): PET fiber, (c1) and (c2): HDPE fiber, (a1), (b1), and (c1): collected in air. (a2), (b2), and (c2) collected in an ethanol-filled chamber, and (a3), (b3), and (c3) are edge scattering of fibers.

In order to test our model and better understand the edge scattering of the fibers, simulations with parameter $z = 0$ for the three samples were obtained by using Eq. (3) as shown in Fig. 8. At an ultra-low q region ($q = 0$ nm^{-1} to 0.04 nm^{-1}), the intensity in simulations were set to zero for the sheltering effect of the beam-stop. The edge scattering intensity in the simulation decreases with increasing q (for HDPE and PET fibers, $q < 0.1$; for carbon fiber, $q < 0.2$), which is qualitatively consistent with the experimental data. In Fig. 8(c), the simulation result agrees very well with the experimental data of HDPE fiber. However, for the carbon fiber (Fig. 8(a)), the simulation data gradually deviates from the experimental data as q increases. The major reason appears to be the difference between the electron density of the fiber and ethanol. In Table 1, we can see that the values of δ for PET and HDPE fibers are close to that of ethanol. According to $\delta \approx \rho \cdot \lambda^2$, it is easy to see that the electron density of carbon fiber is higher than that of PET and HDPE's. This indicates that there is a big contrast in electron density between carbon fiber and ethanol. When the carbon fiber is measured immersed in an ethanol-filled chamber (Fig. 8(a2)), the edge scattering is eliminated only partially, not perfectly. However, for PET and HDPE fibers, the edge scattering was eliminated completely because the contrast of electron density was zero. It is also found that

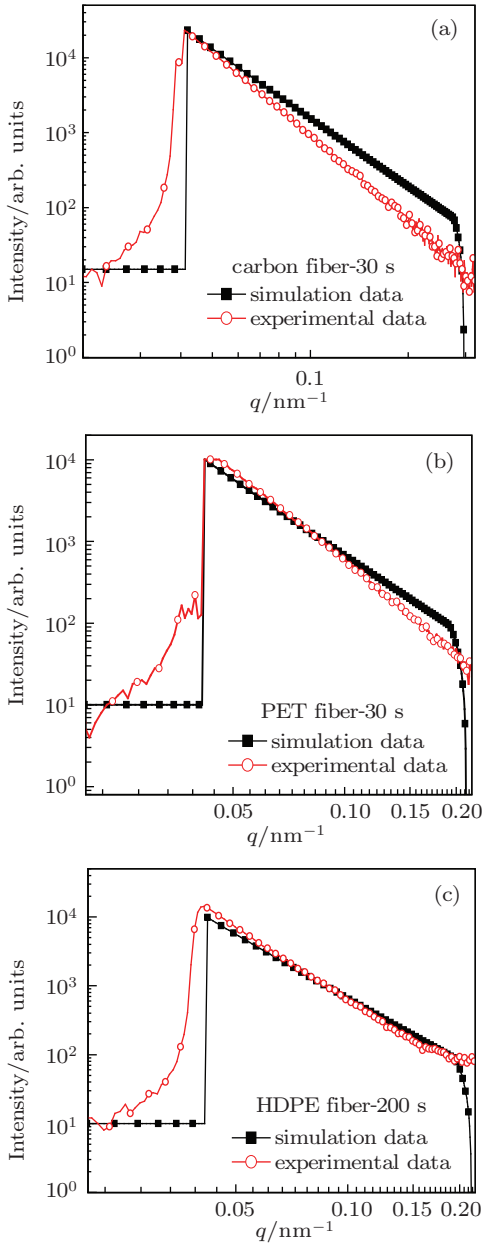


Fig. 8. (color online) Edge scattering in simulation and experiment at $z = 0$ for different fibers. (a) Carbon fiber, (b) PE fiber, (c) HDPE fiber.

the slope of the simulation result is in agreement with experimental data for HDPE, but for PET fiber (whose electron density equals that of ethanol), there is a distinct angle between the simulation result and the experimental data. In our case, it might come from the surface roughness of the fiber sample. The fibers were assumed to be smooth cylinders in our simulation model, somewhat different from the surface of real fibers. Because the surface roughness of our experimental samples affects the scattering intensity,[28] simulation data values can be expected to be larger than experimental data values.

4. Conclusions

In this study, SAXS experiments were performed to investigate edge scattering for different fibers and a new data analysis method for edge scattering of fibers was proposed. In our experiments, for the cylindrical fibers, when measured in ethanol, intensity is dramatically lower in the equatorial streak compared to measurements in air. Weak or even no equatorial streaks were found in the roughly index-matching fluid. This indicates that edge scattering is very strong and can be eliminated or weakened in experiments.

In our simulation, edge scattering from the surface of a cylindrical fiber is best described as refraction. Edge scattering intensity is strong and makes an important contribution to the equatorial streak. Two factors influence edge scattering intensity. One is the sample-to-detector distance (D); edge scattering intensity increases with increasing D. This may explain some unexpected results, such as the finding that the equatorial streak is weak or even disappears when the sample-to-detector distance is shortened. The other is the refraction index. For different samples, the absorption of X-rays is different, and the edge scattering makes different contributions to the equatorial streak. It should be emphasized that edge scattering is a dominant factor but it is not the only factor in equatorial streak. Comparing simulation data and experimental data, it was found that the simulation data are basically consistent with the experimental data. So after eliminating the edge scattering, the intrinsic scattering information of the fibers can be obtained.

Acknowledgment

The authors acknowledge Prof. Ma Jing-Hong and Dr. Gao Xue-Ping for providing the samples. They are also grateful to Zhou Ping and Hong Chu-Xia of the BL16B1 beamline in SSRF for assistance during SAXS experiments.

References

[1] Hong X G, Du L C, Ye M P and Weng Y X 2004 *Chin. Phys.* **13** 720
[2] Han F T, Chen J Z and Wang J Q 1995 *Chin. Phys.* **4** 204
[3] Li Z H, Gong Y J, Zhang Y, Wu D, Sun Y H, Liu Y and Dong B Z 2001 *Chin. Phys.* **10** 429
[4] Wang D H, Hao J J, Xing X Q, Mo G, Gong Y, Lü C X and Wu Z H, 2011 *Chin. Phys.* C **35** 870
[5] Müller M, Czihak C, Vogl G, Fratzl P, Schober H and Riekel C 1998 *Macromolecules* **31** 3953
[6] Diana G S 2006 *J. Appl. Polym. Sci.* **100** 1067
[7] Statton W O 1962 *J. Polym. Sci.* **58** 205
[8] Reimschuessel A C and Prevorsek D C 1976 *J. Polym. Sci. Part B: Polym. Phys.* **14** 485
[9] Sakaoku K, Morosoff N and Peterlin A 1973 *J. Polym. Sci. Part B: Polym. Phys.* **11** 31
[10] Thünemann A F and Ruland W 2000 *Macromolecules* **33** 1848
[11] Perret R and Ruland W 1969 *J. Appl. Crystallogr.* **2** 209
[12] Wang W J, Murthy S N, Chae H G and Kumar S 2009 *J. Polym. Sci., Part B: Polym. Phys.* **47** 2394
[13] Takaku A and Shioya 1986 *J. Mater. Sci.* **21**, 4443
[14] Kaburagi M, Bin Y Z, Zhu D, Xu C Y and Matsuo M 2003 *Carbon* **41** 915
[15] Jiang G S, Huang W F, Li L, Wang X, Pang F J, Zhang Y M and Wang H P 2012 *Carbohydrate Polymers* **87** 2012
[16] Jiang G S, Yuan Y, Wang B C, Yin X M, Mukuze K S, Huang W F, Zhang Y M and Wang H P 2012 *Cellulose* **19** 1075
[17] Janosi A, Grosse I and Hermel G 1996 *Mon. Chem.* **127** 143
[18] Kitagawa T, Murase H and Yabuki K 1998 *J. Polym. Sci.: Part B: Polym. Phys.* **36** 39
[19] Grubb D T, Prasad K and Adams W 1991 *Polymer* **32** 1167
[20] Ran S F, Fang D F, Zong X, Hsiao B S, Chu B and Cunniff P M 2001 *Polymer* **42** 1601
[21] Ran S F, Zong X, Fang D F, Hsiao B S, Chu B, Cunniff P M and Phillips R A 2001 *J. Mater. Sci.* **36** 3071
[22] Wu J, Schultz J M, Yeh F J, Hsiao B S and Chu B 2000 *Macromolecules* **33** 1765
[23] Grubb D T and Murthy N S 2010 *Macromolecules* **43** 1016
[24] Davies R J, Koenig C, Burghammer M and Riekel C 2008 *Appl. Phys. Lett.* **92** 101903
[25] Li X Y, Li X H, Wang Y Z and Wang J 2011 *Adv. Mater. Res.* **332–334** 1171
[26] Hentschel M P, Hosemann R, Lange A and Bruckner R 1987 *Acta Crystallogr.* **A43** 506
[27] Harbich K W, Klobes P and Hentschel M P 2004 *Colloids and Surface A: Physicochem. Eng. Aspects* **241** 225
[28] Gupta A, Harrsion I R and Lahijani J 1994 *J. Appl. Crystallogr* **27** 627
[29] http://henke.lbl.gov/optical_constants/getdb2.html
[30] Rungswang W, Kotaki M, Shimojima T, Kimura G, Sakurai S and Chirachanchai S 2011 *Polymer* **52** 844